ARCHIVE OF MECHANICAL ENGINEERING

DOI: 10.24425/ame.2026.158904 2026, Vol. 73, No. 2, pp. 267–288

Jaime GALLARDO-ALVARADO [1], Mario A. GARCIA-MURILLO [2]

Kinematics of 3-PRS parallel manipulators with integrated parasitic motions via screw theory

Received 24 December 2025, **Revised** 05 May 2026, **Accepted** 14 May 2026, **Published online** 11 June 2026

Keywords: equivalent axis, parasitic motion, 2R1T motion, screw theory, zero-torsion mechanism

Kinematic behavior of a 3-PRS parallel manipulator is investigated with particular emphasis on the characterization and analysis of the so-called parasitic motions. These unintended displacements, arising from the mechanism's inherent geometric and structural constraints, play a critical role in determining the overall accuracy and performance of parallel manipulators. The displacement analysis is performed using two distinct strategies based on simple closure equations, enabling the derivation of expressions for the parasitic displacements of the moving platform. Subsequently, the input-output velocity relationship is obtained by applying the theory of screws. This expression is independent of passive joint rates and can be directly applied to both inverse and forward velocity analyses. Numerical examples, validated using specialized software such as ADAMS,™are presented to demonstrate that the so-called parasitic motions are both predictable and computable, rather than the result of unexpected or random behavior in the zero-torsion mechanism.

1. Introduction

The introduction of Gough's hexapod [1] as a testing platform for tire durability under varying load conditions represented a pivotal milestone in the evolution of modern parallel kinematics. This innovative mechanism not only demonstrated the practical potential of parallel manipulators but also highlighted their superiority in terms of structural rigidity, compactness, and precision when compared to traditional serial manipulators.

However, the complexity of its kinematic behavior, particularly the challenge of direct position analysis, posed significant theoretical and computational diffi-

✉ Jaime GALLARDO-ALVARADO, email: jaime.gallardo@itcelaya.edu.mx

[1]National Technological Institute of Mexico, Celaya, Mexico.

[2]University of Guanajuato, Salamanca, Mexico.

culties. This problem sparked a sustained wave of research aimed at developing new classes of parallel manipulators with alternative topologies. The goal was to preserve the fundamental advantages of the six-legged parallel manipulator while simplifying the mathematical treatment of its kinematics, thereby enabling more efficient modeling, control, and application.

Over time, these efforts have led to the design of manipulators with reduced computational burden, improved workspace characteristics, and enhanced adaptability to industrial and scientific applications. As a result, the Gough hexapod not only stands as a landmark in mechanical design but also as the catalyst for an entire research domain dedicated to advancing parallel robotics and expanding its practical utility across diverse fields such as aerospace, automotive engineering, and precision manufacturing.

Amid the diverse landscape of alternative manipulators, one finds the so-called zero-torsion mechanisms [2]. These mechanical devices are distinguished by possessing three degrees of freedom, traditionally understood to grant the moving platform the capacity for a translation normal to the plane of the fixed platform, accompanied by two rotations within that same plane. Put simply, the moving platform is theoretically restricted from performing any lateral displacement.

Nevertheless, in practical applications, the mobility of the moving platform is not always as idealized in theory. It can be influenced by lateral displacements, which manifest as unintended motions that compromise the precision and reliability of the platform's trajectory. These deviations are often described as unexpected behaviors, leading to inaccuracies and undesirable performance in tasks that demand high fidelity of motion. Thereafter, the term *parasitic motion* emerges to try to explain this phenomenon.

Such observations raise the possibility that the conventional assumption that zero-torsion parallel manipulators are inherently immune to lateral motion may be oversimplified. Rather than dismissing these deviations as mere anomalies, they may instead highlight limitations in the prevailing kinematic models. This suggests that the established kinematic analysis of these manipulators requires careful reconsideration and refinement. A more rigorous and comprehensive framework would not only clarify the true mobility characteristics of the moving platform but also provide engineers and researchers with a more reliable basis for design, control, and practical implementation. Within this context, the development of a comprehensive and reliable kinematic analysis method for zero-torsion parallel manipulators represents an attractive topic.

1.1. Literature survey

Parasitic motion represents a significant kinematic phenomenon in mechanical systems. It arises as an inherent and unavoidable characteristic of lower-mobility parallel mechanisms, where unintended or secondary movements accompany the desired motion. These parasitic displacements, although not part of the primary

functional output, play a crucial role in influencing the accuracy, efficiency, and overall performance of the mechanism. Understanding and analyzing parasitic motion is therefore essential for the design, optimization, and control of parallel mechanisms, particularly in applications requiring high precision such as robotics, machine tools, and motion simulators. There are only a few mechanisms in which motion is not influenced by parasitic effects, for example, the tip-and–ilt motion in a telescope [3]. In other situations, when parasitic motions cannot be entirely eliminated, it is possible to employ a compensation mechanism. Such mechanisms are designed to counteract unwanted disturbances by introducing corrective motions or adjustments [4]. Another approach documented in the specialized literature consists of employing redundant actuation frameworks, as exemplified by the nanorobotics manipulator proposed in [5] or in a manipulator used for rehabilitation proposed by Liang [6]; nevertheless, this approach heightens the complexity of both the mechanical design and the control architecture.

Three-legged parallel manipulators with three degrees of freedom, in which the moving platform is connected to the limbs through spherical joints, were first introduced by Merlet [7]. Parallel manipulators capable of executing 2R1T motion (two rotational and one translational degree of freedom) have attracted significant research interest, with the 3-PRS parallel manipulator being one of the most extensively studied configurations. The 2R1T motion is widely used in robotics and parallel mechanisms because it allows precise orientation control combined with linear movement, making it especially valuable in surgical robots, manipulators, and compact parallel mechanisms. Moreover, such architectures are extensively utilized within medical contexts, most notably in lower-extremity rehabilitation robotics [8–10]. The study of these motions is not merely a kinematic exercise but a fundamental requirement for clinical safety and therapeutic efficacy: for instance, note that the human ankle-joint complex does not possess a fixed center of rotation. Saglia et al [11] emphasize that any rehabilitation device must accommodate the natural shifting of the ankle's axis. If parasitic motions are not accurately modeled, they can lead to a severe misalignment between the robot and the anatomical joint. Misalignment induces unwanted reaction forces and moments on the ligaments. Uncompensated parasitic translations can result in shear stresses that may jeopardize the recovery of injured tissues or cause discomfort to the patient. To ensure that therapy follows the prescribed physiological ranges of motion (dorsiflexion/plantarflexion and inversion/eversion), the control system must compensate for parasitic displacements. Failure to do so "contaminates" the exercise, transforming a pure rotational task into a complex multi-axial movement that the patient may not be prepared to perform [9].

Carretero et al [12] defined parasitic motions in 3-PRS parallel manipulators as unintended displacements occurring in three unspecified motion coordinates, arising from constraint equations that govern the inter-relationships among six motion coordinates. Fan et al [13] conducted a sensitivity analysis with respect to the structural parameters of the 3-PRS parallel kinematic spindle platform in

a five-degree-of-freedom serial-parallel machine tool. Li and Xu [14] derived a closed-form solution for the inverse displacement problem of 3-PRS parallel manipulators, whereas the forward kinematics, an even more challenging problem, was addressed using numerical methods. Li and Xu [15] analyzed the mobility of the manipulator using reciprocal screw theory. Subsequently, they addressed the inverse-forward kinematics problem considering the general arrangement of the actuators. The characteristics of the reachable workspace and dexterity, such as kinematic manipulability and the global dexterity index, were derived by varying the layout angle of the actuators.

Herrero et al [16] investigated the influence of parasitic motions on the dynamics of 3-PRS parallel manipulators and subsequently addressed the robot's inverse kinematics. Vallés et al [17] developed a parallel rehabilitation robot based on the 3-PRS topology, in which an orthopedic boot equipped with a force sensor is mounted on the moving platform of the robot to facilitate therapeutic exercises for injured ankles. Yuan and Tsai [18] introduced a decomposition-based strategy to formulate the dynamic model of the 3-PRS parallel manipulator, assuming that the constraint forces imposed by holonomic constraints generate no net force or torque capable of affecting the motion of the moving platform. Ruiz et al [19] present the kinematic design of a 3-PRS compliant parallel manipulator under the assumption of small displacements. The rigid-body kinematics of the robot is analyzed by addressing both the inverse and forward kinematic problems, and by determining the rotations required at the revolute and spherical flexure joints.

Nigatu et al [20] obtain the parasitic-motion equation for a 3-PRS parallel manipulator. The derivation is carried out from the velocity-level analytic constraint equation. By explicitly linking parasitic motion to these velocity-level constraints, the analysis provides a framework for identifying unintended displacements that arise due to the inherent coupling of the system's degrees of freedom. Rao [21] reports an error analysis of the positional parameters in a 3-PRS manipulator. The study determines design parameters, such as orientation, position, location, and the directions of revolute and spherical joints, incorporating design constraints previously defined. Yao et al [22] analyzed two 3-PRS parallel manipulators with distinct branch-chain configurations. Using MATLAB, they derived equations to compute parasitic motions and demonstrated their dependence on structural and kinematic parameters. Zhang et al [23] proposed a feed-rate scheduling method for 3-PRS parallel manipulators that ensures the velocities and accelerations of the drive axes remain within predefined limits by employing screw theory. The approach was subsequently applied to a virtual double-pendulum five-axis serial machine tool.

This study presents a kinematic analysis of the 3-PRS parallel manipulator, with particular emphasis on the analysis of the parasitic motions, a mechanism classified within the 2R1T motion category.

1.2. Organization of the paper

The remainder of this paper is organized as follows. Section *Geometry of the parallel manipulator* describes the architecture and dimensional parameters of the 3-PRS parallel manipulator, along with the closure equations relevant to its kinematic formulation. Section Displacement Analysis derives expressions for computing the lateral displacements of the moving platform's center, based on the mobility constraints of the robot's limbs. In this section, one algorithm is presented for solving the inverse position problem, while another algorithm is proposed for addressing the forward displacement analysis.

Section *Velocity analysis* investigates the instantaneous kinematics of the manipulator using screw theory. The input-output velocity equation, relating the velocity state or twist about a screw of the moving platform with the generalized or input velocities, is derived without dependence on passive joint rates by exploiting the properties of reciprocal screws through the Klein form.

The robustness and reliability of the proposed kinematic analysis are demonstrated in Section *Numerical application* through the solution of illustrative numerical examples. The results obtained via screw theory are further validated using an alternative approach, specifically through the application of specialized software such as ADAMS.™

Finally, the paper concludes with a summary of findings and key insights.

2. Geometry of the parallel manipulator

The architecture of the parallel manipulator under study is depicted in Fig. 1. It comprises a moving platform, denoted by m, connected to a fixed platform, denoted by 0, through three PRS-type limbs, in which the prismatic joints (underlined) are actuated. Each limb is attached to the fixed platform via an active prismatic joint and connected to the moving platform through a passive spherical joint.

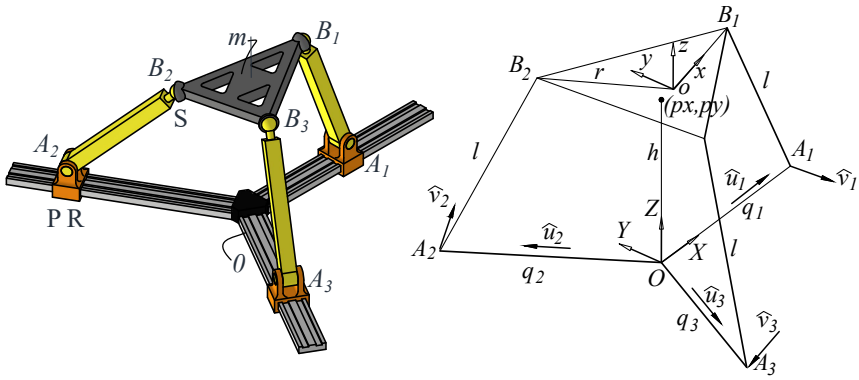

Fig. 1. The 3-RPS parallel manipulator. Topology and dimensional parameters

To describe the topology and dimensional parameters of the robot, one defines a reference frame O_XYZ fixed to the base, with the $Z-$axis oriented normal to the plane of the fixed platform.

Prismatic and revolute joints are combined to form compound joints, whose kinematic behavior is defined through a set of characteristic points A_i, with $i = 1, 2, 3$. These points serve as reference markers that describe the relative motion and constraints imposed by the lower kinematic pairs. The position vectors $\boldsymbol{a}_i$ of points A_i are calculated as:

$$\boldsymbol{a}_i = q_i \hat{\boldsymbol{u}}_i \quad i = 1, 2, 3, \tag{1}$$

where $\hat{\boldsymbol{u}}_i$ is the $i-$th unit vector describing the orientation of the $i-$th compound joint on the fixed platform. Indeed,

$$\hat{\boldsymbol{u}}_1 =< 1, 0, 0 >, \hat{\boldsymbol{u}}_2 =< -1/2, \sqrt{3}/2, 0 >, \hat{\boldsymbol{u}}_3 =< -1/2, -\sqrt{3}/2, 0 > . \tag{2}$$

Meanwhile, q_i denotes the $i-$th linear generalized coordinate associated to the $i-$th actuated prismatic joint.

Similarly, the orientation of the revolute joints is specified by the unit vectors $\hat{\boldsymbol{v}}_i (i = 1, 2, 3)$, defined as follows:

$$\hat{\boldsymbol{v}}_1 =< 0, -1, 0 >, \hat{\boldsymbol{v}}_2 =< -\sqrt{3}/2, -1/2 >, \hat{\boldsymbol{v}}_3 =< \sqrt{3}/2, -1/2 > . \tag{3}$$

Naturally, $\hat{\boldsymbol{u}}_i \cdot \hat{\boldsymbol{v}}_i = 0$ for $i = 1, 2, 3$.

The moving platform forms an equilateral triangle with vertices B_1, B_2, and B_3 inscribed in a circle of radius r and center o. Then, the centers of the spherical joints are positioned at the vertices B_1, B_2, and B_3. A reference frame o_xyz is attached to the moving platform, where the $z-$axis is oriented normal to the plane of the moving platform, and the $x-$axis points from the origin o toward point B_1. In this context, the coordinates of the centers of the spherical joints expressed in the moving reference frame are defined as follows:

$$b_1 = (r, 0, 0), \; b_2 = (-r/2, \sqrt{3}r/2, 0), \; b_3 = (-r/2, -\sqrt{3}r/2, 0).$$

In this context, the parameter l represents the fixed distance that separates point B_i from point A_i.

To specify the orientation of the moving reference frame relative to the fixed reference frame, let $\hat{\boldsymbol{k}} = (k_X, k_Y, k_Z)$ denote the equivalent axis of a finite rotation, where the unit vector $\hat{\boldsymbol{k}}$ is expressed in the fixed frame. If θ represents the rotation angle of the frame o_xyz about the axis $\hat{\boldsymbol{k}}$, then the rotation matrix $\boldsymbol{R}$ relating the two reference frames is given by [24]:

$$\boldsymbol{R} = \begin{bmatrix} k_X k_X v\theta + c\theta & k_X k_Y v\theta - k_Z s\theta & k_X k_Z v\theta + k_Y s\theta \\ k_X k_Y v\theta + k_Z s\theta & k_Y k_Y v\theta + c\theta & k_Y k_Z v\theta - k_X s\theta \\ k_X k_Z v\theta - k_Y s\theta & k_Y k_Z v\theta + k_X s\theta & k_Z k_Z v\theta + c\theta \end{bmatrix}, \tag{4}$$

where, for brevity, $c\theta = \cos\theta$, and $s\theta = \sin\theta$, and $v\theta = 1 - \cos\theta$. However, owing to the condition of zero-torsion mechanism, it follows that $k_Z = 0$.

To facilitate the manipulation of trigonometric expressions, it is advisable to consider the tangent half-angle ζ as follows:

$$\zeta = \tan\theta/2, \quad \sin\theta = 2\zeta/(1+\zeta^2), \quad \cos\theta = (1-\zeta^2)/(1+\zeta^2). \tag{5}$$

On the other hand, a compact representation of matrix $\boldsymbol{R}$ is offered in the formulation proposed by Gallardo-Alvarado et al [25], expressed as:

$$\boldsymbol{R} = \left[\hat{\boldsymbol{u}} \quad \hat{\boldsymbol{w}} \quad \hat{\boldsymbol{u}} \times \hat{\boldsymbol{w}}\right], \tag{6}$$

where the unit vectors $\hat{\boldsymbol{u}}$ and $\hat{\boldsymbol{w}}$ are defined as follows:

$$\hat{\boldsymbol{u}} = (\boldsymbol{b}_1 - \boldsymbol{o})/r, \quad \hat{\boldsymbol{w}} = (\boldsymbol{b}_2 - \boldsymbol{b}_3)/\sqrt{3}r. \tag{7}$$

In other words, the unit vector $\hat{\boldsymbol{u}}$ is aligned with the $x-$axis, whereas the unit vector $\hat{\boldsymbol{w}}$ is aligned with the $y-$axis. The vector $\hat{\boldsymbol{u}}$, $\hat{\boldsymbol{w}}$ and $\hat{\boldsymbol{u}} \times \hat{\boldsymbol{w}}$ form an orthogonal basis that characterizes the orientation of the moving platform within the space.

Assuming that

$$\boldsymbol{R} = \begin{bmatrix} r_{11} & r_{12} & r_{13} \\ r_{21} & r_{22} & r_{23} \\ r_{31} & r_{32} & r_{33} \end{bmatrix}, \tag{8}$$

then

$$\theta = \arccos\left(\frac{r_{11} + r_{22} + r_{33} - 1}{2}\right), \tag{9}$$

and

$$\hat{\boldsymbol{k}} = \frac{1}{2\sin\theta} < r_{32} - r_{23}, r_{13} - r_{31}, r_{21} - r_{12} > . \tag{10}$$

The coordinates of the centers of the spherical joints expressed in both reference frames are related as follows:

$$B_i = \boldsymbol{o} + \boldsymbol{R}\ b_i \quad i = 1, 2, 3, \tag{11}$$

where $\boldsymbol{o}$ is the position vector of point o with respect to point O. Furthermore, since the moving platform exhibits the shape of an equilateral triangle then it follows that

$$o = (B_1 + B_2 + B_3)/3. \tag{12}$$

Meanwhile, the angle θ is determined as:

$$\theta = 2 \arctan \zeta. \tag{13}$$

The relevant closure equations governing the kinematic behavior of the parallel manipulator can be expressed as follows. These equations establish the geometric constraints that must be satisfied for the mechanism to maintain its configuration. In particular, from the definition of the parameter l, it follows that

$$(\boldsymbol{b}_i - \boldsymbol{a}_i) \cdot (\boldsymbol{b}_i - \boldsymbol{a}_i) = l^2 \quad i = 1, 2, 3. \tag{14}$$

On the other hand, the revolute joints restrict the location of the spherical joint centers in such a manner that

$$(\boldsymbol{b}_i - \boldsymbol{a}_i) \cdot \hat{\boldsymbol{v}}_i = 0 \quad i = 1, 2, 3. \tag{15}$$

Meanwhile, along the sides of the equilateral triangle $\Delta B_1 B_2 B_3$, three closure equations can be formulated as follows:

$$(\boldsymbol{b}_1 - \boldsymbol{b}_2) \cdot (\boldsymbol{b}_1 - \boldsymbol{b}_2) = 3r^2, \tag{16a}$$

$$(\boldsymbol{b}_2 - \boldsymbol{b}_3) \cdot (\boldsymbol{b}_2 - \boldsymbol{b}_3) = 3r^2, \tag{16b}$$

$$(\boldsymbol{b}_1 - \boldsymbol{b}_3) \cdot (\boldsymbol{b}_1 - \boldsymbol{b}_3) = 3r^2. \tag{16c}$$

3. Displacement analysis

The objective of the displacement analysis of the parallel manipulator is to derive a mathematical formulation that links the pose of the moving platform m, with the set of generalized coordinates q_i for $i = 1, 2, 3$. This relationship provides the foundation for describing the kinematic behavior of the mechanism, enabling the determination of the platform's position and orientation as functions of the joint variables and vice versa.

3.1. Parasitic motions

Lateral displacements of the center o of the moving platform are commonly classified as parasitic motions, since they represent unintended deviations from the desired trajectory. These motions occur when the platform experiences small but significant shifts perpendicular to its primary direction of movement, thereby introducing errors into the system's kinematic behavior. In precision mechanisms, such as parallel manipulators or robotic platforms, parasitic motions are undesirable because they reduce accuracy, compromise stability, and may lead to misalignment between the moving platform and its intended path.

To compute the parasitic motions, we assume that $k_Z = 0$ in the rotation matrix $\boldsymbol{R}$, see Eq. (4). Moreover, we define the position vector as $\boldsymbol{o} = (p_x, p_Y, h)$, where

p_x and p_Y represent the parasitic motions while h is the elevation of the moving platform.

For limb labeled 1, by applying Eq. (15), we obtain that

$$(\boldsymbol{b}_1 - \boldsymbol{a}_1) \cdot \hat{\boldsymbol{v}}_1 = 0. \tag{17}$$

Hence, after a few computations it follows that

$$p_Y = -k_X \, k_Y \, r \, (1 - \cos\theta), \tag{18}$$

where $k_X^2 + k_Y^2 = 1$. Through an equivalent procedure, the formulation obtained from limb 2 or limb 3 is:

$$p_X = r(k_X^2 - k_Y^2)(1 - \cos\theta)/2. \tag{19}$$

It is worth noting that p_X and p_Y depend on the radius r of the moving platform. Consequently, one cannot guarantee that these lateral displacements are small [12, 26]. For example, provided that $k_Y^2 = 1 - k_X^2$, considering a reference radius of $r = 100$ [mm] for the moving platform, together with the variation of the component k_X of the equivalent axis $\hat{\boldsymbol{k}}$ in the range $-1 \leq k_X \leq 1$, and the angle θ restricted to $-\pi/3 \leq \theta \leq \pi/3$ [rad], the resulting plots illustrating the parasitic displacements of the center o of the moving platform are presented in Fig. 2.

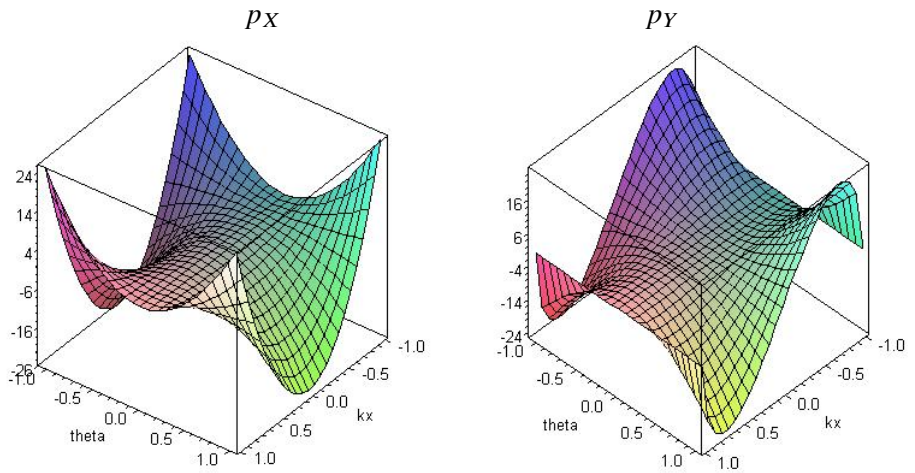

Fig. 2. Plots of the parasitic motions. The plots show that the lateral displacements correspond to 25% of the parameter r, which constitutes a significant deviation

This subsection demonstrates that the so-called parasitic motions are not incidental anomalies but rather intrinsic consequences of the underlying topology of the zero-torsion mechanism. Specifically, the lateral displacements of the moving platform are inherently coupled to the system's geometry and vanish simultaneously

only in the singular case when $\theta = 0$. This observation highlights that parasitic motions are neither random disturbances nor unforeseen imperfections; instead, they are systematic, predictable, and fully computable within the kinematic framework. Their deterministic nature suggests that the conventional terminology of *parasitic* may be misleading, as it implies accidental or undesirable behavior. A more precise nomenclature could acknowledge their structural origin and emphasize their role as an inherent characteristic of the mechanism rather than an extraneous defect.

3.2. Inverse displacement analysis

The inverse displacement analysis involves determining the generalized coordinates that correspond to a prescribed pose of the moving platform. In this context, it is important to consider that the zero-torsion mechanism was originally designed with the moving platform restricted to both lateral displacements and rotations oriented normal to its plane. In other words, the mechanism's conception confines the moving platform to execute a 2R1T motion (two rotations and one translation). From the perspective of inverse displacement analysis, the 2R1T motion is attainable in zero-torsion mechanisms solely through the inclusion of parasitic motions. Thus, in general, the translational motion of the center o of the moving platform is not perpendicular to the plane of the fixed platform, contrary to the traditional assumption.

The inverse displacement analysis can be formulated as follows: Given the pose of the moving platform relative to the fixed platform, the objective is to determine the generalized coordinates q_i for $i = 1, 2, 3$. The procedure for performing the inverse displacement analysis can be summarized in the following steps:

1. Select the pose of the moving platform based on the unit vector $\hat{\boldsymbol{k}}$, the angle θ, and the parameter h;
2. Compute the parasitic motions p_X and p_Y;
3. Consider $\boldsymbol{o} = (p_X, p_Y, h)$;
4. Compute the rotation matrix $\boldsymbol{R}$, see Eq. (4);
5. Compute the coordinates of points $B_i (i = 1, 2, 3)$, see Eq. (11);
6. Compute the position vectors $\boldsymbol{a}_i (i = 1, 2, 3)$, see Eq. (1);
7. Determine the generalized coordinates $q_i (i = 1, 2, 3)$ based on Eq. (14).

At the conclusion of the algorithm, each generalized coordinate can be determined by solving a simple quadratic equation. Consequently, up to eight distinct configurations of the parallel manipulator may correspond to a given pose of the moving platform.

3.3. Forward displacement analysis

The forward displacement analysis refers to the process of determining the pose of the moving platform relative to the fixed platform. This analysis is carried out by solving for the moving platform configuration that satisfies a prescribed set

of generalized coordinates q_i, where $i = 1, 2, 3$. In technical terms, the forward displacement analysis consists of computing the center o of the moving platform, the equivalent axis $\hat{\boldsymbol{k}}$, and the finite rotation θ given the generalized coordinates $q_i (i = 1, 2, 3)$.

The underlying algorithm for forward displacement analysis can be systematically structured through the following steps:

1. Select a set of generalized coordinates $q_i (i = 1, 2, 3)$;
2. Define $\boldsymbol{o} =< p_X, p_Y, h >$ and $\hat{\boldsymbol{k}} =< k_X, k_Y, k_Z >$;
3. Compute the coordinates of points $A_i (i = 1, 2, 3)$, see Eq. (1);
4. Define the trigonometric identities

$$\sin\theta = \frac{2\zeta}{1+\zeta^2}, \quad \cos\theta = \frac{1-\zeta^2}{1+\zeta^2}, \quad v\theta == \frac{2\zeta^2}{1+\zeta^2};$$

5. Compute the rotation matrix $\boldsymbol{R}$ using Eq. (4);
6. Determine the centers of the spherical joints through Eq. (11);
7. Formulate three non-linear equations from Eqs. (15) as follows

$$[(\boldsymbol{b}_i - \boldsymbol{a}_i) \cdot \hat{\boldsymbol{v}}_i]\ (1+\zeta^2) = 0 \quad i = 1, 2, 3;$$

8. According to Eqs. (14), three non-linear equations are written as follows

$$[(\boldsymbol{b}_i - \boldsymbol{a}_i) \cdot (\boldsymbol{b}_i - \boldsymbol{a}_i) - l^2](1+\zeta^2)^2 = 0 \quad i = 1, 2, 3;$$

9. The seventh equation follows from the fact that $\hat{\boldsymbol{k}}$ is a unit vector, satisfying $\hat{\boldsymbol{k}} \cdot \hat{\boldsymbol{k}} = 1$;
10. Thereafter, seven non-linear equations in the unknowns p_X, p_Y, h, k_X, k_Y, k_Z, and ζ are available for solving the forward displacement analysis problem;
11. The system of seven non-linear equations is resolved numerically, for instance using the Newton-homotopy method. In that concern one obtains $k_Z = 0$;
12. Compute θ as $\theta = 2 \arctan\zeta$;
13. Compute point o as $\boldsymbol{o} =< p_X, p_Y, h >$ and $\hat{\boldsymbol{k}} =< k_X, k_Y, 0 >$;
14. Compute the rotation matrix $\boldsymbol{R}$ using Eq. (4);
15. Determine the centers of the spherical joints, points $B_i (i = 1, 2, 3)$, through Eq. (11);
16. Compute the unit vectors $\hat{\boldsymbol{u}}$ and $\hat{\boldsymbol{w}}$ according to Eqs. (7).

The position of the moving platform is described by the position vector $\boldsymbol{o}$. Its orientation, in turn, can be represented by the unit vectors $\hat{\boldsymbol{u}}$ and $\hat{\boldsymbol{v}}$. Alternatively, the orientation of the moving platform may be defined by the unit vector $\hat{\boldsymbol{k}}$ and the angle θ. On the other hand, reducing the seven non-linear equations to a single univariate polynomial lies beyond the scope of this paper. Therefore, the Newton-homotopy method is employed to obtain the real solutions. In this context, the forward displacement analysis yields at most eight solutions, excluding reflected configurations.

4. Velocity analysis

In this section, the velocity analysis of the parallel manipulator is conducted using screw theory [27], a powerful mathematical framework that unifies the representation of linear and angular motion and is isomorphic to motor algebra [28]. This methodology provides an elegant and systematic foundation for kinematic modeling. By leveraging the geometric properties of screws, the instantaneous motion of each manipulator component can be characterized with greater precision, facilitating the derivation of a compact and geometrically insightful input-output velocity equation.

The velocity state of a rigid body, commonly referred to as the twist about a screw, for the moving platform m relative to the fixed platform 0, is formally defined within screw theory as the union of two fundamental components: (i) the angular velocity vector ${}^0\boldsymbol{\omega}^m$, which characterizes the rotational motion of the moving platform, and (ii) the linear velocity vector $\boldsymbol{v}_Q$, representing the translational velocity of an arbitrary point Q rigidly attached to the platform named the reference pole. This inseparable coupling of rotational and translational motion is expressed as a six-dimensional vector ${}^0\boldsymbol{V}_Q^m$, which compactly encapsulates the complete instantaneous motion of the platform in a geometrically meaningful form. Mathematically, the velocity state of the rigid body is given by:

$$ {}^0\boldsymbol{V}_Q^m = \begin{bmatrix} {}^0\omega^m \\ \boldsymbol{v}_Q \end{bmatrix}. \tag{20} $$

The velocity state of a rigid body can be elegantly represented in screw theory format, which provides a unified framework for describing both translational and rotational motion. Within the context of parallel manipulators, this representation is particularly powerful, as it allows the kinematic contribution of each individual limb to be considered independently. By formulating the velocity state limb by limb, one can perform a localized analysis of the characteristics of the motion of the moving platform while still maintaining consistency with the overall kinematic structure of the manipulator.

This limb-wise formulation is valid for every chain of the mechanism, thereby enabling a systematic decomposition of the platform's instantaneous motion into contributions from its constituent limbs. A crucial concept in this framework is that of reciprocal screws. These elements play a fundamental role in eliminating the influence of passive joint rates, ensuring that the velocity state reflects only the effective motion transmitted through the zero-torsion mechanism. In other words, reciprocal screws act as filters that nullify passive joint motions, thereby preserving the integrity of the kinematic description.

The interplay between screws and reciprocal screws provides deep insight into the manipulator's instantaneous mobility and constraint characteristics. Their geometric representation offers a clear visualization of how motion and constraint

spaces interact, which is invaluable for both theoretical analysis and practical design. The screws and their corresponding reciprocal screws are illustrated in Fig. 3.

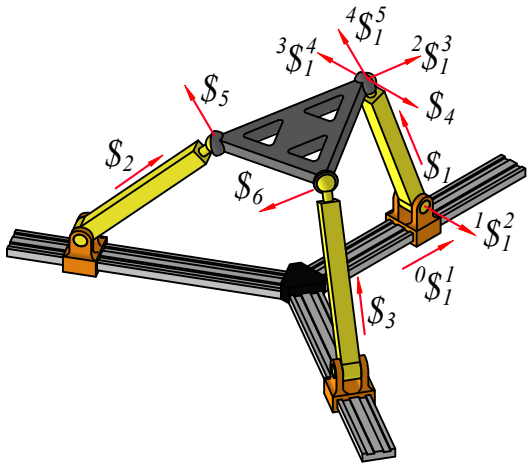

Fig. 3. Screws of the 3-PRS parallel manipulator

By selecting the origin O of the fixed reference frame as the reference pole, the velocity state of the moving platform can be expressed in screw format through any of the limbs of the parallel manipulator as follows:

$$ {}^0\boldsymbol{V}_O^m = \dot{q}_i \; {}^0\$_i^1 + {}_1\omega_2^i \; {}^1\$_i^2 + {}_2\omega_3^i \; {}^2\$_i^3 + {}_3\omega_4^i \; {}^3\$_i^4 + {}_4\omega_5^i \; {}^4\$_i^5 \quad i = 1, 2, 3. \tag{21} $$

The experience obtained through displacement analysis demonstrates that parasitic motions cannot be neglected when modeling the kinematic behavior of the system. To achieve a complete and accurate representation, these parasitic motions must be incorporated into the velocity state. Consequently, the velocity state should be expressed as a six-dimensional vector, encompassing both the intended and unintended motion components. In this framework, six reciprocal screws are required to establish the input-output velocity relationship of the parallel manipulator. This formulation ensures that the manipulator's kinematic model captures the full spectrum of motion interactions, thereby providing a more robust basis for subsequent analysis, control, and optimization.

Let us consider the reciprocal screws $\$_i (i = 1, 2, 3)$. By systematically applying the Klein form, denoted as $\{*;*\}$, to both sides of Eq. (21) and simplifying the resulting expressions, one obtains:

$$ \left\{\$_i; {}^0\boldsymbol{V}_O^m\right\} = \dot{q}_i \left\{\$_i; {}^0\$_i^1\right\} \quad i = 1, 2, 3. \tag{22} $$

Similarly, by resorting to the reciprocal screws $\$_i (i = 4, 5, 6)$ it follows that

$$\{\$_i; {}^0\boldsymbol{V}_O^m\} = 0 \quad i = 4, 5, 6. \tag{23}$$

To further streamline the formulation, Eqs. (22) and (23) can be recast into a matrix-vector format. This representation not only enhances clarity but also facilitates the systematic treatment of the kinematic relations. In particular, the resulting expression isolates the active degrees of freedom, thereby yielding an input-output velocity relationship that is independent of passive joint rates. The elimination of these passive terms underscores the efficiency of the matrix formulation, as it highlights the direct mapping between the actuated inputs and the corresponding output velocities, expressed as:

$$\boldsymbol{J}\,\boldsymbol{\Delta}\,{}^0\boldsymbol{V}_O^m = \boldsymbol{C}\,\boldsymbol{Q}v, \tag{24}$$

where:

$\boldsymbol{J} = \begin{bmatrix} \$_1 & \$_2 & \$_3 & \$_4 & \$_5 & \$_6 \end{bmatrix}$ is the Jacobian matrix of the manipulator;

$\boldsymbol{\Delta} = \begin{bmatrix} \mathbf{O} & \boldsymbol{I} \\ \boldsymbol{I} & \mathbf{O} \end{bmatrix}$ is the polarity operator which is formed with the zero matrix $\mathbf{O}$ and the identity matrix $\boldsymbol{I}$;

$\boldsymbol{C} = \text{diag}\begin{bmatrix} \{\$_1; {}^0\$_1^1\} & \{\$_2; {}^0\$_2^1\} & \{\$_3; {}^0\$_3^1\} & 0 & 0 & 0 \end{bmatrix}$ is the first-order coefficient matrix of the robot;

$\boldsymbol{Q}v = \begin{bmatrix} \dot{q}_1 & \dot{q}_2 & \dot{q}_3 & \dot{q}_4 & \dot{q}_5 & \dot{q}_6 \end{bmatrix}^T$ is the first-order driver matrix of the parallel manipulator in which $\dot{q}_i = 0$ for $i = 4, 5, 6$, are virtual generalized velocities introduced with the purpose to satisfy an algebraic requirement.

5. Numerical simulation

This section presents a set of numerical simulations derived from the kinematic analysis of the parallel manipulator. The primary objective is to validate the analytical model and assess its robustness under diverse operating conditions. These simulations demonstrate the practical applicability and reliability of the proposed kinematic framework. For this purpose, the parameters of the 3-PRS parallel manipulator are selected as $r = 100$ [mm] and $l = 200$ [mm].

Inverse displacement

Let us consider that the pose of the moving platform m is such that the equivalent axis is given by $\hat{\boldsymbol{k}} =< 0.8, 0.6, 0 >$ endowed with a finite rotation $\theta = 0.15$ [rad]. Furthermore, let us consider that the height of the moving platform is given by $h = 170$ [mm].

According to Eqs. (19) and (18), the parasitic motions are obtained as:

$$p_X = 0.157 \text{ [mm]}, \quad p_Y = -0.538 \text{ [mm]}.$$

Subsequently, the coordinates of the centers $B_i (i = 1, 2, 3)$ [mm] of the spherical joints are determined as:

$$\begin{cases} B_1 = (99.752, 0, 161.033) \\ B_2 = (-49.173, 85.171, 184.836) \\ B_3 = (-50.107, -86.788, 164.129) \end{cases}.$$

Afterwards, the generalized coordinates $q_i (i = 1, 2, 3)$ [mm] are computed, yielding the complete set of parameters that fully describe the configuration of the system as:

$$q_1 = \begin{cases} 218.362 \\ -18.856 \end{cases} \quad q_2 = \begin{cases} 174.737 \\ 21.957 \end{cases} \quad q_3 = \begin{cases} 214.501 \\ -14.071 \end{cases}$$

Selecting one solution of the inverse displacement analysis, we define the robot's reference configuration using the data presented in Table 1.

Table 1. Reference configuration of the robot

limb	q_i [mm]	A_i [mm]	B_i [mm]
1	218.362	(218.362,0,0)	(99.752,0,161.033)
2	174.737	(-87.368,151.327,0)	(-49.173,85.171,184.836)
3	214.501	(-107.250,-185.763,0)	(-50.107,-86.688,164.129)
$p_X = 0.157$ [mm]	$p_Y = -0.538$ [mm]	$h = 170$ [mm]	$\theta = 0.15$ [rad]

Forward displacement

Let us consider the solution of the inverse displacement problem where the generalized coordinates were obtained as $q_1 = 218.362$ [mm], $q_2 = 174.737$ [mm] and $q_3 = 214.501$ [mm]. Using this set of generalized coordinates, the forward position algorithm was applied, yielding, excluding reflected solutions, the results presented in Table 2.

Solution 2 in Table 2 has been identified as the reference configuration for the robot. This configuration serves as the baseline posture from which subsequent analyses and simulations are conducted.

Velocity

In the reference configuration of the robot, see Table 1, the generalized coordinates are prescribed to evolve according to periodic functions of time. Specifically,

Table 2. The eight real solutions of the forward displacement analysis

sol.	$\boldsymbol{o}$ [mm]	$\hat{\boldsymbol{k}}$	θ [rad]
1	<-25.395,-4.462,131.869>	<0.086,0.996,0>	1.065
2	<0.157,-0.538,170>	<0.8,0.6,0>	0.150
3	<17.879,20.763,129.849>	<0.908,-0.416,0>	1.101
4	<21.313,-35.696,113.324>	<-0.869,-0.493,0>	1.401
5	<-25.395,-4.462,131.869>	<-0.086,-0.996,0>	-1.065
6	<0.157,-0.538,170>	<-0.8,-0.6,0>	-0.150
7	<17.879,20.763,129.849>	<-0.908,0.416,0>	-1.101
8	<21.313,-35.696,113.324>	<0.869,0.493,0>	-1.401

the motion is defined by the following expressions:

$$q_1 = 100 \sin t \cos t \ [\text{mm}], \ \ q_2 = 200 \sin t \cos t \ [\text{mm}], \ \ q_3 = 80 \sin t \cos t \ [\text{mm}],$$

where the independent variable t denotes time, restricted to the interval $0 \leq t \leq 2\pi$ [s].

These functions describe oscillatory trajectories for the generalized coordinates q_1, q_2, and q_3. Since each coordinate is expressed as a product of sine and cosine terms, the resulting motion corresponds to a sinusoidal pattern with a fundamental period of 2π seconds. The amplitudes differ across coordinates, with q_1, q_2, and q_3 scaled by factors of 100, 200, and 80 millimeters, respectively, thereby producing distinct magnitudes of oscillation while maintaining synchronized temporal behavior. In addition to the numerical results of the instantaneous kinematics, the example also considers relevant results from the displacement analysis as a necessary intermediate step.

The equivalent axis $\hat{\boldsymbol{k}} =< k_X, k_Y, k_Z >$ plays a pivotal role in the characterization of zero-torsion mechanisms. Its time evolution is illustrated in Fig. 4.

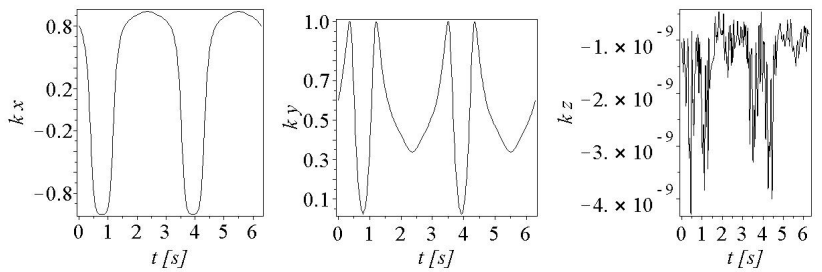

Fig. 4. Temporal evolution of the equivalent axis $\hat{\boldsymbol{k}}$. Notably, the component k_Z vanishes, thereby conferring the designation of zero-torsion mechanism to the 3-PRS parallel manipulator

Meanwhile, the time history of the angle θ is provided in Fig. 5.

The temporal evolution of the kinematic behavior of the moving platform taking point o as the reference pole is illustrated in Figs. 6, 7, and 8, where the response

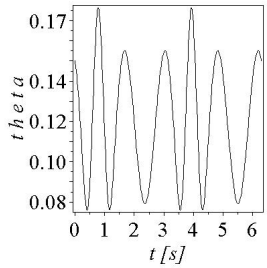

Fig. 5. Temporal evolution of the angle θ

of the system can be observed in detail. To ensure the reliability and accuracy of the numerical results obtained through the application of screw theory, a virtual prototype of the 3-PRS parallel manipulator was developed and simulated using ADAMS™software. This modeling environment allows for a realistic representation of the manipulator's motion and provides a robust framework for validating theoretical predictions.

For a comprehensive comparison between both approaches, the plots generated through ADAMS™simulations are systematically positioned beneath the corresponding results derived from screw theory. This arrangement facilitates a direct visual and analytical evaluation of the consistency between the theoretical formulation and the numerical simulation, thereby reinforcing the validity of the proposed methodology.

It is particularly noteworthy that the results obtained through the application of screw theory exhibit excellent agreement with those generated using ADAMS™. This consistency between two fundamentally different methodologies underscores the robustness of the theoretical framework and the reliability of the simulation environment. At this juncture, however, a natural and thought-provoking question arises: if parasitic motions in zero-torsion mechanisms are inherently unpredictable and manifest as unexpected deviations from ideal behavior, how can it be that identical numerical results are produced when employing both approaches?

The agreement between screw theory and ADAMS™does not imply that parasitic motions are eliminated, but rather that both methodologies are capable of capturing the intrinsic behavior of the mechanism within their respective modeling paradigms. This convergence of results reinforces confidence in the validity of the theoretical analysis and highlights the complementary role of simulation in validating complex kinematic phenomena.

6. Conclusions

Traditionally, zero-torsion mechanisms are described as possessing three fundamental degrees of freedom: a single translational motion oriented perpendicular to the plane of the fixed platform, accompanied by two rotational motions confined

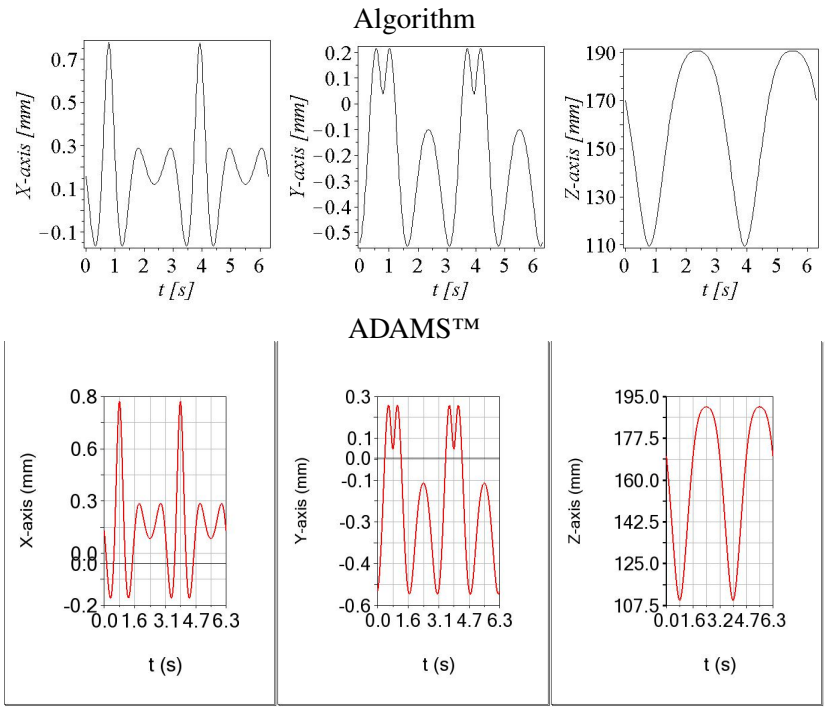

Fig. 6. Temporal evolution of the position vector of the center o of the moving platform. The parasitic motions p_X and p_Y correspond to the X and Y axes, respectively

within the plane of the fixed platform [12, 26]. This simplified characterization has long been accepted in the literature and serves as the basis for modeling and control strategies.

However, practical implementations have revealed that the moving platform of these mechanisms does not always conform strictly to this idealized behavior. In reality, the moving platform can exhibit lateral displacements that deviate from the expected motion set. These displacements, often referred to as *parasitic motions*, have historically been considered undesirable, unexpected, and even arbitrary, as if they were anomalies or imperfections in the manipulator's performance [12, 20, 29].

For example, note that, as illustrated in Figure 2, the lateral displacements reach approximately 25% of the platform radius (r). These values represent a significant magnitude that cannot be disregarded in the kinematic analysis, given their detrimental impact on operational accuracy, especially in high-precision fields such as medical robotics or industrial machining. Consequently, this mandates the use of robust control strategies to effectively compensate for these deviations.

This paper shows that parasitic motions are neither random nor accidental. Instead, they are intrinsic to the topology and geometry of the manipulator itself. Far from being unpredictable, these motions arise naturally from the kinematic constraints imposed by the mechanism's structure. Consequently, they can be sys-

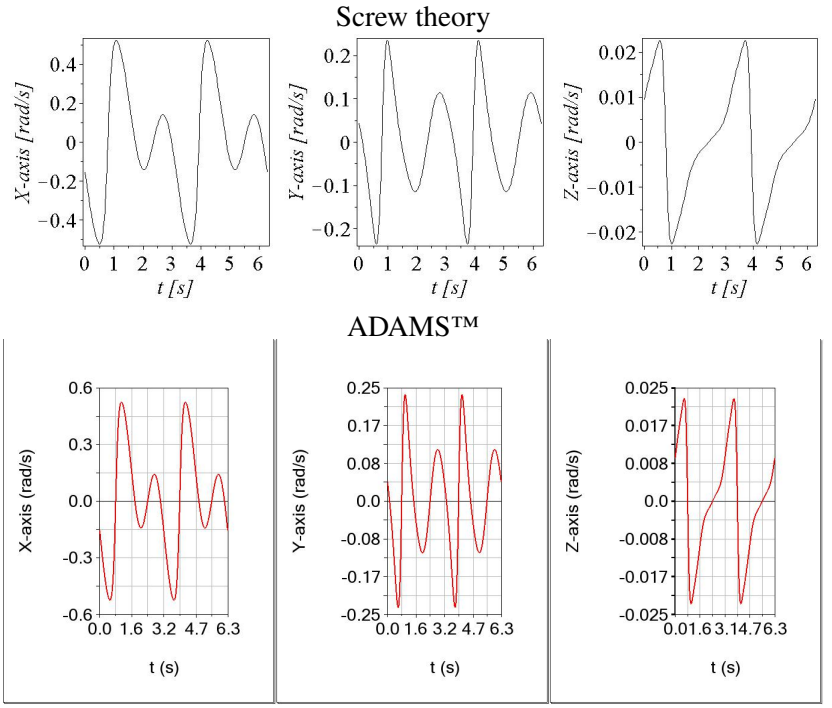

Fig. 7. Temporal evolution of the angular velocity vector of the moving platform. Although $k_Z = 0$ at all times, a parasitic angular velocity persists along the $Z-$axis

tematically analyzed, modeled, and quantified. The mechanism chosen for the analysis is the 3-PRS parallel manipulator.

The principal findings of this study can be synthesized and articulated as follows:

1. Expressions for calculating the parasitic motions of the moving platform are derived from the constraint assembly of the robot's limbs. These motions depend on the circumradius of the moving platform and, therefore, cannot be assumed to be small [12, 26];
2. Except for the special case in which the finite rotation θ vanishes, the 3-PRS robot exhibits parasitic motions, the presence of such motions is virtually inescapable;
3. The nomenclature 2R1T+1Rp2Tp, where Rp and Tp denote parasitic motions, provides a more descriptive representation of a zero-torsion mechanism;
4. The inverse displacement analysis reveals that there are up to eight different configurations of the 3-PRS parallel manipulator given the pose of the moving platform;

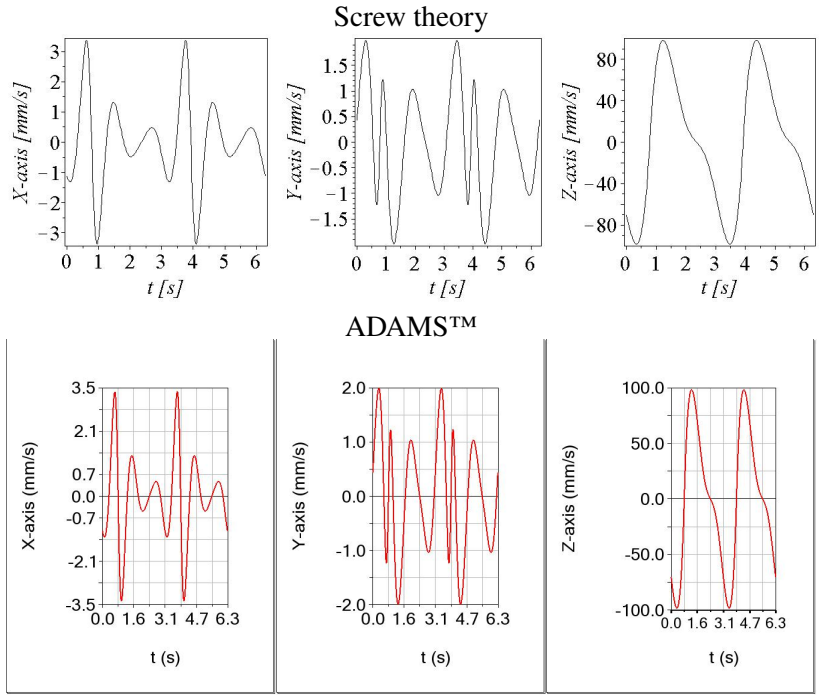

Fig. 8. Temporal evolution of the velocity vector of the center o of the moving platform

5. The forward displacement analysis leads to seven non-linear equations. The numerical results show that the vertical component k_Z of the equivalent axis $\hat{\boldsymbol{k}}$ vanishes;
6. The input-output velocity equation relating the velocity state of the moving platform with the generalized velocities is obtained free of passive joint rates;
7. The parasitic motions are incorporated into the kinematic analysis. Consequently, the velocity state is represented as a six-dimensional vector. However, this does not imply an increase in the robot's degrees of freedom, since the parasitic motions remain dependent on the three generalized coordinates of the robot;
8. Numerical examples, which are verified using an alternative strategy such as the application of special software like ADAMS™, are provided to demonstrate the robustness and reliability of the method of kinematic analysis developed in the paper;
9. The 3-PRS parallel manipulator undergoes three parasitic motions, comprising one rotational and two translational components.

Finally, the methodology presented in this paper for addressing the kinematic analysis of the 3-PRS parallel manipulator can be readily generalized to other zero-torsion mechanisms. This extrapolation requires no substantial modifications,

thereby highlighting the versatility and broader applicability of the proposed approach within the field of parallel robotics.

References

[1] V.E. Gough. Contribution to discussion of papers on research in automobile stability. In *Proceedings of the Automobile Division of the Institution of Mechanical Engineers*, volume 171, pages 392–394, 1957.

[2] I.A. Bonev. Direct kinematics of zero-torsion parallel mechanisms. In *2008 IEEE International Conference on Robotics and Automation*, pages 3851–3856, 2008. doi: 10.1109/ROBOT.2008.4543802.

[3] J.A. Carretero, M. Nahon, B. Buckham, and C.M. Gosselin. Kinematic analysis of a three-DOF parallel mechanism for telescope applications. In *International Design Engineering Technical Conferences and Computers and Information in Engineering Conference*, volume Volume 2: 23rd Design Automation Conference, page V002T29A008, 1997. doi: 10.1115/DETC97/DAC-3981.

[4] A. Ruiz, F.J. Campa, C. Roldan-Paraponiaris, O. Altuzarra, and C. Pinto. Experimental validation of the kinematic design of 3-PRS compliant parallel mechanisms. *Mechatronics*, 39:77–88, 2016. doi: 10.1016/j.mechatronics.2016.08.006.

[5] H. Yu and P. Yan. A 3-dof redundant parallel mechanism without parasitic motion for spatial nanopositioning. *IEEE Access*, 13:66468–66477, 2025. doi: 10.1109/ACCESS.2025.3561029.

[6] X. Liang, X. Zeng, G. Li, T. Su, and G. He. Kinematic analysis of three redundant parallel mechanisms for fracture reduction surgery. *Mechanism and Machine Theory*, 188:105400, 2023. doi: 10.1016/j.mechmachtheory.2023.105400.

[7] J.-P. Merlet. *Parallel Robots*. Solid Mechanics and Its Applications. Springer Dordrecht, 2006. doi: 10.1007/1-4020-4133-0.

[8] M.G. Alvarez-Perez, M.A. Garcia-Murillo, and J.J. Cervantes-Sanchez. Robot-assisted ankle rehabilitation: a review. *Disability and Rehabilitation: Assistive Technology*, 15(4):394–408, 2020. doi: 10.1080/17483107.2019.1578424.

[9] M. Valles, J. Cazalilla, A. Valera, V. Mata, A. Page, and M. Diaz-Rodriguez. A 3-prs parallel manipulator for ankle rehabilitation: towards a low-cost robotic rehabilitation. *Robotica*, 35(10):1939–1957, 2017. doi: 10.1017/S0263574715000120.

[10] V.E. Abarca and D.A. Elias. A review of parallel robots: Rehabilitation, assistance, and humanoid applications for neck, shoulder, wrist, hip, and ankle joints. *Robotics*, 12(5):131, 2023. doi: 10.3390/robotics12050131.

[11] J.A. Saglia, N.G. Tsagarakis, J.S. Dai, and D.G. Caldwell. A high performance 2-dof over-actuated parallel mechanism for ankle rehabilitation. In *2009 IEEE International Conference on Robotics and Automation*, pages 2180–2186, 2009. doi: 10.1109/ROBOT.2009.5152604.

[12] J.A. Carretero, R.P. Podhorodeski, M.A. Nahon, and C.M. Gosselin. Kinematic analysis and optimization of a new three degree-of-freedom spatial parallel manipulator. *Journal of Mechanical Design*, 122(1):17–24, 1999. doi: 10.1115/1.533542.

[13] K.C. Fan, H. Wang, J.W. Zhao, and T.-H. Chang. Sensitivity analysis of the 3-PRS parallel kinematic spindle platform of a serial-parallel machine tool. *International Journal of Machine Tools and Manufacture*, 43(15):1561–1569, 2003. doi: 10.1016/S0890-6955(03)00202-5.

[14] Y. Li and Q. Xu. Kinematics and inverse dynamics analysis for a general 3-PRS spatial parallel mechanism. *Robotica*, 23(2):219–229, 2005. doi: 10.1017/S0263574704000797.

[15] Y. Li and Q. Xu. Kinematic analysis of a 3-PRS parallel manipulator. *Robotics and Computer-Integrated Manufacturing*, 23(4):395–408, 2007. doi: 10.1016/j.rcim.2006.04.007.

[16] S. Herrero, C. Pinto, J. Corral, and O. Altuzarra. Actuators orientation influence in the energy consumption of the 3-PRS manipulator. In *ASME International Mechanical Engineering Congress and Exposition*, volume Volume 4B: Dynamics, Vibration and Control, page V04BT04A071, 2013. doi: 10.1115/IMECE2013-63166.

[17] M. Valles, J. Cazalilla, A. Valera, V. Mata, A. Page, and M. Diaz-Rodriguez. A 3-PRS parallel manipulator for ankle rehabilitation: towards a low-cost robotic rehabilitation. *Robotica*, 35(10):1939–1957, 2017. doi: 10.1017/S0263574715000120.

[18] W.-H. Yuan and M.-S. Tsai. A novel approach for forward dynamic analysis of 3-PRS parallel manipulator with consideration of friction effect. *Robotics and Computer-Integrated Manufacturing*, 30(3):315–325, 2014. doi: 10.1016/j.rcim.2013.10.009.

[19] A. Ruiz, F.J. Campa, C. Roldan-Paraponiaris, O. Altuzarra, and C. Pinto. Experimental validation of the kinematic design of 3-PRS compliant parallel mechanisms. *Mechatronics*, 39:77–88, 2016. doi: 10.1016/j.mechatronics.2016.08.006.

[20] H. Nigatu, Y.H. Choi, and D. Doik Kim. Analysis of parasitic motion with the constraint embedded jacobian for a 3-PRS parallel manipulator. *Mechanism and Machine Theory*, 164:104409, 2021. doi: 10.1016/j.mechmachtheory.2021.104409.

[21] P.S. Rao. Calibrating a synthesized 3-PRS manipulator by minimizing the errors in positions of revolute joints. *Journal of The Institution of Engineers (India): Series C*, 103:1083–1093, 2022. doi: 10.1007/s40032-022-00866-0.

[22] Y. Yao, W. Wu, R. Li, and Y. Zhao. Parasitic motions of 3-PRS parallel mechanisms with two different branch chain arrangements. *Applied Sciences*, 13:5425, 2023. doi: 10.3390/app13095425.

[23] H. Zhang, J. Yang, S. Gao, X. Gong, and W. Zhu. Feedrate scheduling method for 3-PRS hybrid machine tools considering kinematic constraints. *Robotics and Computer-Integrated Manufacturing*, 95:102988, 2025. doi: 10.1016/j.rcim.2025.102988.

[24] J.J. Craig. *Introduction to Robotics, Global Edition*. Pearson Education, 2021.

[25] J. Gallardo-Alvarado, C.R. Aguilar-Najera, L. Casique-Rosas, L. Perez-Gonzales, and J.M. Rico-Martinez. Solving the kinematics and dynamics of a modular spatial hyper-redundant manipulator by means of screw theory. *Multibody System Dynamics*, 20:307–325, 2008. doi: 10.1007/s11044-008-9121-7.

[26] J. Carretero, M. Nahon, and R. Podhorodeski. Workspace analysis and optimization of a novel 3-DOF parallel manipulator. *International Journal of Robotics and Automation*, 15:178–188, 12 2000. doi: 10.3390/su3112217.

[27] J. Gallardo-Alvarado. *Kinematic Analysis of Parallel Manipulators by Algebraic Screw Theory*. Springer, Cham, 2016. doi: 10.1007/978-3-319-31126-5.

[28] R. von Mises. *Motor Calculus: A New Theoretical Device for Mechanics*. Institute for Mechanics, University of Technology, 1996.

[29] Y. Liu, L. Wang, J. Wu, and J. Wang. A comprehensive analysis of a 3-P (Pa) S spatial parallel manipulator. *Frontiers of Mechanical Engineering*, 10:7–19, 2015. doi: 10.1007/s11465-015-0324-3.